

## PAPER



Cite this: *J. Mater. Chem. B*, 2017,  
5, 9546

## Targeted delivery of a guanidine-pendant Pt(IV)-backboned poly-prodrug by an anisamide-functionalized polypeptide†

Shao-Lu Li, <sup>‡,ab</sup> Yaoyi Wang, <sup>‡,b</sup> Jingfang Zhang, <sup>b</sup> Wei Wei\*<sup>c</sup> and Hua Lu <sup>\*b</sup>

We describe here a novel targeting polyion complex (Tg-PIC) system for the delivery and intracellular release of cisplatin. Briefly, a guanidinium-pendant Pt(IV)-backboned poly-prodrug termed P(DSP-Gu) is prepared with excellent aqueous solubility, high drug-loading and high potency. To enable prolonged circulation and selective cellular internalization, P(DSP-Gu) is complexed with anisamide-end-capped poly(ethylene glycol)-*block*-poly(L-phosphotyrosine)-*block*-poly(L-leucine) (AA-PEG-PpY-PLeu) to yield Tg-PIC *via* electrostatic coacervation. Tg-PIC is stabilized by hydrogen bonding between phosphate and guanidinium, the PEG corona, and the helical poly(L-leucine) segment forming the hydrophobic core. The anisamide group, a high affinity ligand recognizing the sigma ( $\sigma$ ) receptors that are overexpressed on many human malignancies including prostate cancer, is incorporated at the surface of the Tg-PIC for active targeting and efficient internalization. *In vitro*, the Tg-PICs show targeted and efficient internalization into sigma receptor-positive PC3 cells, and can release toxic Pt(II) species due to the degradation of P(DSP-Gu) under the intracellular reducing conditions. *In vivo*, the Tg-PICs exhibit superior antitumor efficacy with reduced toxicity. Thus, the system holds considerable promise towards more effective and safe nanomedicine.

Received 20th September 2017,  
Accepted 15th November 2017

DOI: 10.1039/c7tb02513k

rsc.li/materials-b

## Introduction

The past two decades have witnessed the explosive development of various nanomedicines for cancer.<sup>1–4</sup> To ensure satisfactory efficacy and reduced toxicity, it is necessary to deliver therapeutic cargos to the right place and at the right time. To achieve this goal, nanomedicines have been sophisticatedly designed to overcome biological barriers at various levels and equipped with intelligent properties at different physiological and pathological interfaces.<sup>5–14</sup> Ideally, delivery systems are expected to remain stealthy before encountering the malignant sites, be effectively and selectively internalized by pathological cells, and rapidly release their cargos once inside the targeted cells. These requirements

have posed considerable challenges for designing effective nanomedicines, and many of them fail to accomplish their mission.<sup>14–21</sup> For example, polyion complexes (PICs) generated by electrostatic interactions of two oppositely charged poly-electrolytes have been routinely exploited for nucleic acid and drug delivery; however, many PICs cannot even survive in PBS, not to mention the harsh conditions of plasma.<sup>22–24</sup> Moreover, once inside the cells, the release of cargos from the PICs is often suboptimal to achieve sufficient therapeutic efficacy.<sup>25–29</sup> Nanomedicines with modulable characteristics and responsive properties under different biological environments are therefore highly desirable.<sup>30–34</sup>

Herein, we designed a novel targeting polyion complex (Tg-PIC) system for the *in vivo* delivery and intracellular release of cisplatin, a well-known toxic chemotherapeutic drug.<sup>35–41</sup> Briefly, a guanidinium-pendant Pt(IV)-backboned poly-prodrug termed P(DSP-Gu) was prepared with excellent aqueous solubility, high drug-loading, and high potency. To enable prolonged circulation and selective cellular internalization, P(DSP-Gu) was complexed with anisamide-capped poly(ethylene glycol)-*block*-poly(L-phosphotyrosine)-*block*-poly(L-leucine) (AA-PEG-PpY-PLeu) to yield Tg-PIC *via* electrostatic coacervation (Fig. 1). Tg-PIC was stabilized by electrostatic forces and hydrogen bonding between phosphate and guanidinium,<sup>42–44</sup> the PEG corona, and the hydrophobic core formed by the helical poly(L-leucine)

<sup>a</sup> State Key Laboratory of Separation Membranes and Membrane Processes, School of Materials Science and Engineering, Tianjin Polytechnic University, Tianjin 300387, People's Republic of China

<sup>b</sup> Beijing National Laboratory for Molecular Sciences, Center for Soft Matter Science and Engineering, Key Laboratory of Polymer Chemistry and Physics of Ministry of Education, College of Chemistry and Molecular Engineering, Peking University, Beijing 100871, People's Republic of China. E-mail: chemhualu@pku.edu.cn

<sup>c</sup> State Key Laboratory of Biochemical Engineering, Institute of Process Engineering, Chinese Academy of Sciences, Beijing, 10090, People's Republic of China. E-mail: weiwei@ipe.ac.cn

† Electronic supplementary information (ESI) available. See DOI: 10.1039/c7tb02513k

‡ These authors contributed equally.

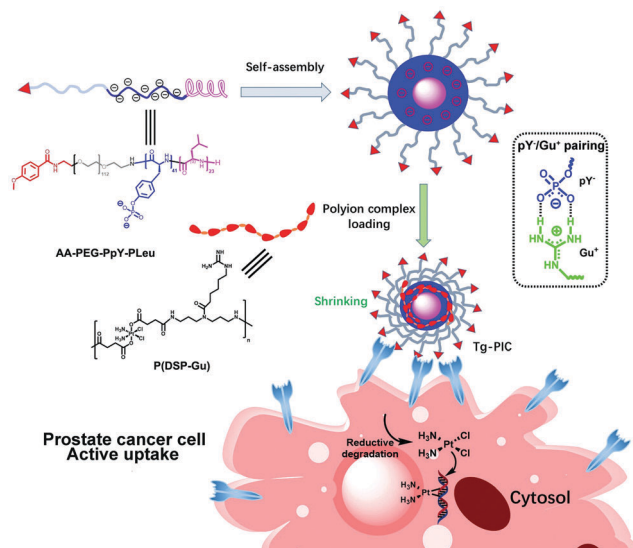


Fig. 1 Chemical structures of AA-PEG-PpY-PLeu and P(DSP-Gu), and schematic illustration of the mechanism of action of Tg-PIC for the targeted delivery of cisplatin.

segment<sup>36,45</sup> (Fig. 1). The anisamide group,<sup>46–52</sup> a high affinity ligand recognizing the sigma ( $\sigma$ ) receptors that are overexpressed on many human malignancies including prostate cancer, was incorporated at the surface of the Tg-PIC for active targeting and efficient internalization. Once inside the tumor cells, the Tg-PIC system is expected to release toxic Pt(II) species due to the degradation of P(DSP-Gu) under the intracellular reducing conditions, and thus achieve selective toxicity.<sup>53,54</sup>

## Results and discussion

### Synthesis and characterization of P(DSP-Gu)

P(DSP-Gu), a fully degradable and highly water soluble Pt(IV)-backboned poly-prodrug, was synthesized as illustrated in Scheme 1. The amine group of 6-aminohexanoic acid was firstly transformed into Boc-protected guanidine to afford **Gu-1**, whose free carboxylic acid was then coupled to **Gu-11** to generate **Gu-2** bearing two trifluoroacetyl amides. After the deprotection of the trifluoroacetyl group from **Gu-2**, a bisamine-functionalized compound **Gu-3** was generated for condensation polymerization with NHS-Pt-NHS, a bifunctional Pt(IV) prodrug. By following a previously described polymerization protocol, the Boc-protected polymer **Gu-4** was produced in high yield. **Gu-4** was then deprotected in TFA and dialyzed at 4 °C (MWCO 3.5 K) to afford the guanidinium-pendant P(DSP-Gu). Here, the guanidinium group was introduced to enhance solubility and facilitate internalization of the Pt(IV)-backboned poly-prodrug.

The purity and identity of the polymer were well characterized using <sup>1</sup>H NMR spectroscopy in both D<sub>2</sub>O (Fig. 2a) and DMSO-*d*<sub>6</sub> (Fig. S9, ESI†). The appearance of a peak at 3.2 ppm, which was attributed to a combination of the methylene proton “b” adjacent to the newly formed amide bond and the methylene proton “c” next to the guanidinium units, indicated the successful generation of the desired product. The purity of P(DSP-Gu) was further

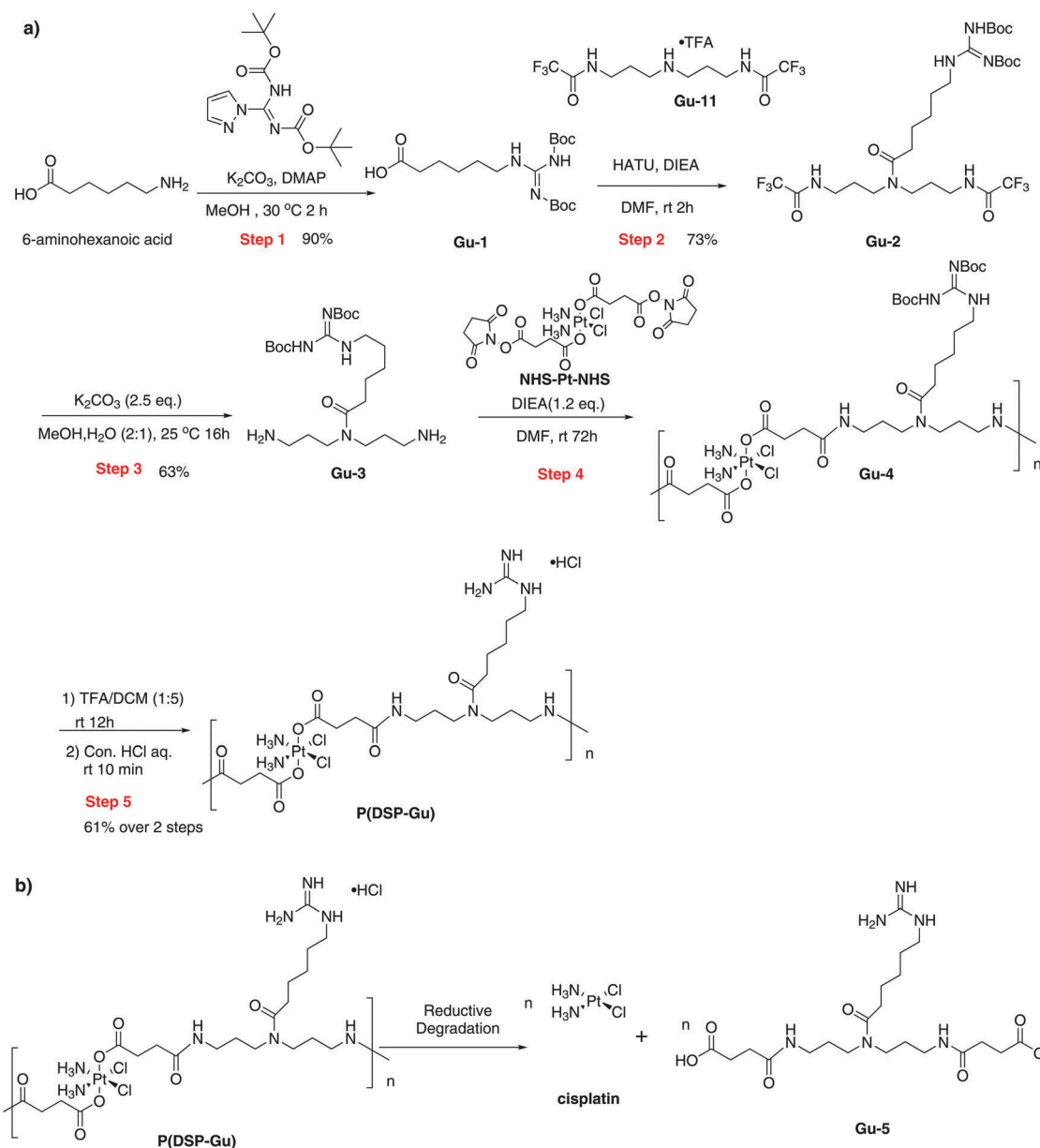
confirmed by the 22.2% Pt content according to ICP-MS measurement, which was in good agreement with the theoretical value of 23.8%. This, by calculation, gave a drug loading as high as 36.5%. The reduction potentials of P(DSP-Gu) at two different physiological pH values (pH 6.0 and 7.4) were recorded by cyclic voltammetry (Fig. 2b and c). Electrochemical studies revealed behavior characteristic of irreversible loss of the Pt(IV) axial ligands. The reductive potential of P(DSP-Gu) was determined to be –118.9 and –82.5 mV at pH 7.4 and 6.0, respectively (Fig. S10a and b, ESI†).<sup>53,55</sup> Thus, this suggested that the acidic environment inside cancer cells could facilitate its reduction. Notably, polymeric P(DSP-Gu) had a higher tendency towards reduction compared to its small molecular analogues, which might be a consequence of the polymeric bulky ligand (a high degree of polymerization).<sup>56–58</sup>

### Synthesis and characterization of AA-PEG-PpY-PLeu

As shown in Scheme 2, the amphiphilic triblock copolymer AA-PEG-PpY-PLeu was synthesized in five steps. Starting from mono-Boc protected bisamine-functionalized PEG (BocNH-PEG-NH<sub>2</sub>), PEG functionalized with an anisamide and an amine on each end (A-2) was generated within two steps. A-2 then served as a macro-initiator for the successive ring-opening polymerization (ROP) of pOEt-Tyr-NCA and Leu-NCA to yield the precursor polymer A-4. The degree of polymerization (DP) of pOEt-Tyr and PLeu, determined by <sup>1</sup>H NMR, was 41 and 23, respectively (Fig. S13, ESI†). The successful construction of A-4 was further demonstrated by gel permeation chromatography (GPC) analysis (Fig. S14, ESI†). AA-PEG-PpY-PLeu was obtained after the deprotection of the ethyl groups by TMSBr/TEA in dry CHCl<sub>3</sub>, followed by extensive dialysis against water. The disappearance of the ethyl peak in the <sup>1</sup>H NMR spectrum of AA-PEG-PpY-PLeu indicated complete and successful deprotection. Peaks “a” and “e” confirmed the presence of the targeting ligand anisamide (Fig. S15, ESI†). A non-targeting polymer, mPEG-PpY-PLeu, was also prepared using a similar method starting from mPEG-NH<sub>2</sub> for comparison purposes (Fig. S16 and S17, ESI†).

### Characterization of Tg-PICs

TEM images of AA-PEG-PpY-PLeu and Tg-PICs confirmed the regular well-dispersed spherical shape of the self-assembled particles, which were ~150 nm and ~90 nm on average in the dry state (Fig. 3a). Notably, the size of AA-PEG-PpY-PLeu was fairly polydispersed in TEM, whereas the sizes of Tg-PICs were more monodispersed. In dynamic light scattering (DLS), the amphiphilic polymer AA-PEG-PpY-PLeu exhibited a hydrodynamic diameter of 230 nm (Fig. 3b). After complexing AA-PEG-PpY-PLeu with P(DSP-Gu) at varied phosphate/guanidinium (P/Gu) ratios, the size of the Tg-PICs shrank to 90 nm in diameter using DLS, accompanied by a substantial decrease in polydispersity (PDI) from above 0.3 to lower than 0.1, which was in good agreement with the TEM observation. This change in size was likely a consequence of the condensation of the two polyelectrolytes in solution (Table S1, ESI†). The discrepancy of size in DLS and TEM could be due to hydration.<sup>59,60</sup> Both AA-PEG-PpY-PLeu and



Scheme 1 (a) Synthesis and (b) reductive degradation of P(DSP-Gu).

Tg-PICs showed high colloidal stability and their sizes did not change for more than a week in both PBS buffer and 10% FBS-1640 medium (Fig. 3b), a characteristic that was key to their *in vivo* application.<sup>13,14</sup> The zeta potential of the Tg-PICs increased gradually from  $-17.50$  to  $-6.26$  mV with an increase in the P/Gu ratio from 1/1 to 1/2 (Fig. 3c).

### Reduction and platinum release of Tg-PICs

Next, we tested the reduction of Tg-PICs by monitoring their hydrodynamic sizes in the presence of ascorbic acid (AsA). By incubating the mixtures at pH 7.4 and 37 °C for 10 h, the sizes of the particles in the reaction mixtures increased from 90 to 170 nm, which was close to the size of AA-PEG-PpY-PLeu (Fig. 4a and b). This coincidence suggested that the Tg-PICs

were restored to AA-PEG-PpY-PLeu due to the reductive degradation of P(DSP-Gu).<sup>61</sup>

To estimate the release kinetics of platinum from the Tg-PICs, we incubated the nanoparticles under both reducing (with GSH) and non-reducing conditions (without GSH) in PBS (pH 7.4, 37 °C). Slow and sustained release of platinum, measured by ICP-MS, was observed for P(DSP-Gu) and Tg-PICs under the non-reducing conditions (Fig. 4c). This result was consistent with a previous study reported by Lippard, Langer and Farokhzad, in which they attributed the release to ester hydrolysis.<sup>62,63</sup> Notably, the release rate of Pt in the Tg-PICs was relatively slower than that of P(DSP-Gu), underscoring the stabilization effect of forming nanoparticles.<sup>64,65</sup> Upon the addition of GSH, all samples underwent considerably faster

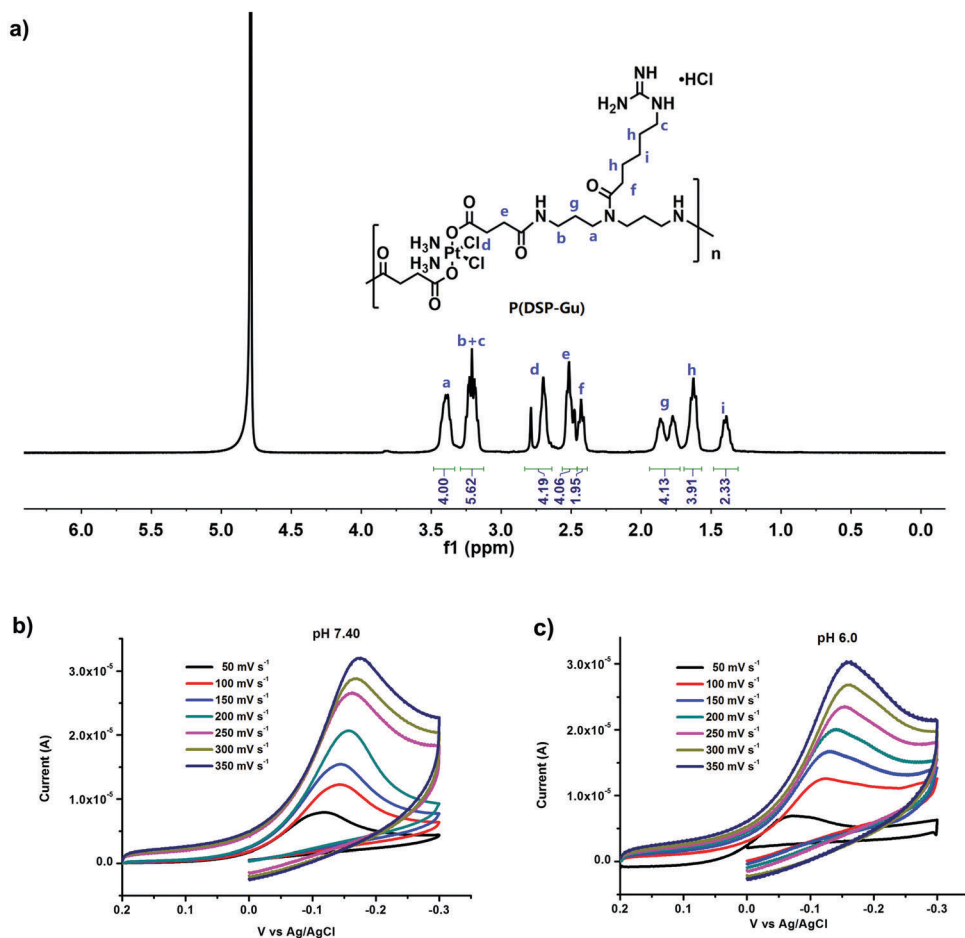


Fig. 2 (a)  $^1\text{H}$  NMR spectrum of P(DSP-Gu) in  $\text{D}_2\text{O}$ . (b and c) Cyclic voltammograms of P(DSP-Gu) in PBS-0.1 M KCl with varied scan rates at pH 7.4 (b) and 6.0 (c).

release of platinum, likely due to the reduction of  $\text{Pt(IV)}$  and the subsequent degradation of P(DSP-Gu). Together, the results suggested that Tg-PICs can achieve spatiotemporal control over drug release. Specifically, our results suggested that P(DSP-Gu) might undergo slow degradation due to ester hydrolysis during circulation, but the majority of Tg-PICs will be rapidly reduced to their active  $\text{Pt(II)}$  form once inside tumor cells.

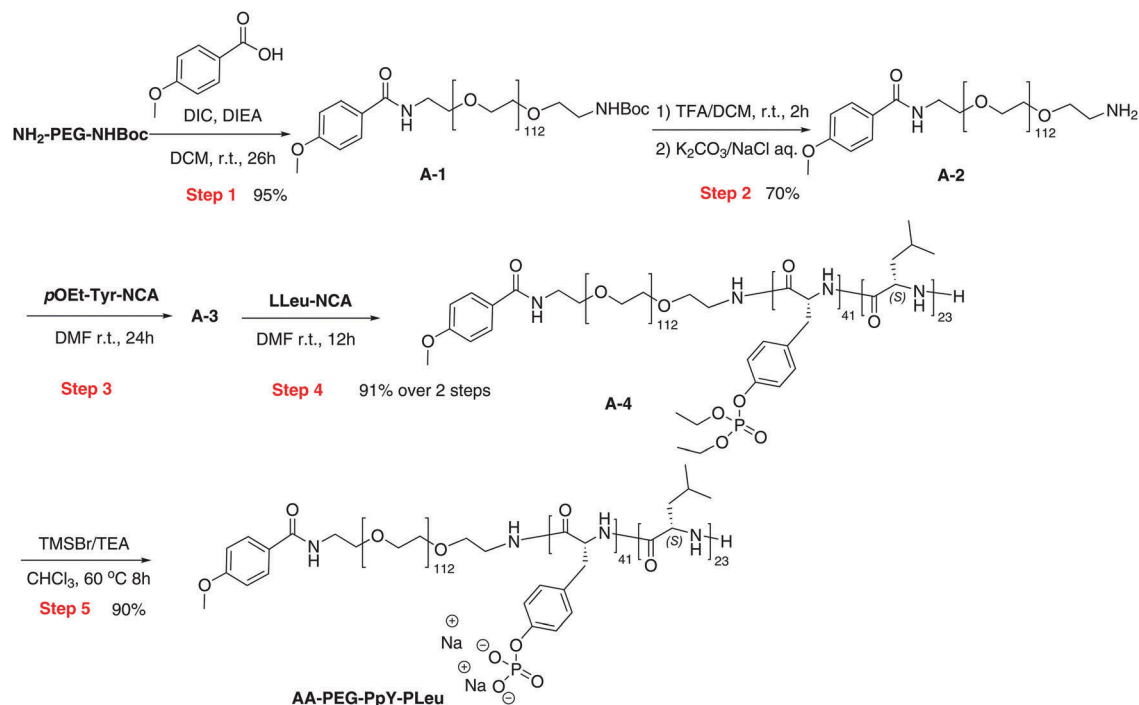
### In vitro cytotoxicity

To examine the cytotoxicity of the carrier polymers AA-PEG-PpY-PLeu and mPEG-PpY-PLeu, the poly-prodrug P(DSP-Gu), and the particles, we performed viability assays by using the human prostate carcinoma cell line PC3, which expresses a high level of the  $\sigma$ -receptor. It was shown that both the targeting AA-PEG-PpY-PLeu and non-targeting mPEG-PpY-PLeu were practically nontoxic to PC3 cells at our tested concentrations ranging from 0.36 to  $800 \mu\text{g mL}^{-1}$ , confirming their excellent biocompatibility (Fig. 5a). The poly-prodrug P(DSP-Gu) showed high anticancer potency with an  $\text{IC}_{50}$  value of  $25 \mu\text{M}$  (based on the concentration of Pt) against PC3 cells, which was slightly less potent than cisplatin ( $\text{IC}_{50}$   $9.9 \mu\text{M}$ ).<sup>62</sup> The  $\text{IC}_{50}$  of Tg-PIC at the P/Gu ratio of 1/1 was estimated to be  $26 \mu\text{M}$ , which was almost identical to that of P(DSP-Gu). In contrast, at the same P/Gu ratio, the  $\text{IC}_{50}$  of

NT-PIC, the analogue PIC based on the non-targeting mPEG-PpY-PLeu and P(DSP-Gu), was  $115 \mu\text{M}$ . Thus, Tg-PIC with an anisamide group was  $\sim 4$  fold more potent than NT-PIC without any targeting ligand (Fig. 5b). Similarly, at the P/Gu ratio of 2/3, Tg-PIC was 2-fold more potent than NT-PIC ( $22 \mu\text{M}$  as compared to  $56 \mu\text{M}$ ) (Fig. S18, ESI<sup>†</sup>). Together, this suggested a ligand-dependent cell toxicity pattern in the sigma receptor-expressing PC3 cells.

### Cellular uptake

To study the cellular uptake of Tg-PIC and NT-PIC in PC3 cells, we labeled P(DSP-Gu) with TAMRA for flow cytometry and confocal laser scanning microscopy (CLSM) experiments. Flow cytometry analysis indicated that Tg-PICs (P/Gu ratios 1/1 and 2/3) were internalized by PC3 cells at appreciably high levels, whereas NT-PICs exhibited much less internalization at the same P/Gu ratio (Fig. 6a and b). Notably, the free polymer P(DSP-Gu) was also efficiently internalized by the cells, likely due to its cationic guanidinium side-chain groups. Moreover, pre-blocking of the  $\sigma$ -receptor of PC3 cells by the antagonist haloperidol led to significant inhibition of internalization of Tg-PICs, further indicating a ligand-dependent cell internalization mechanism.<sup>47,61</sup> The CLSM study also showed similar patterns (Fig. S19, ESI<sup>†</sup>).



Scheme 2 Synthesis of AA-PEG-PpY-PLeu.

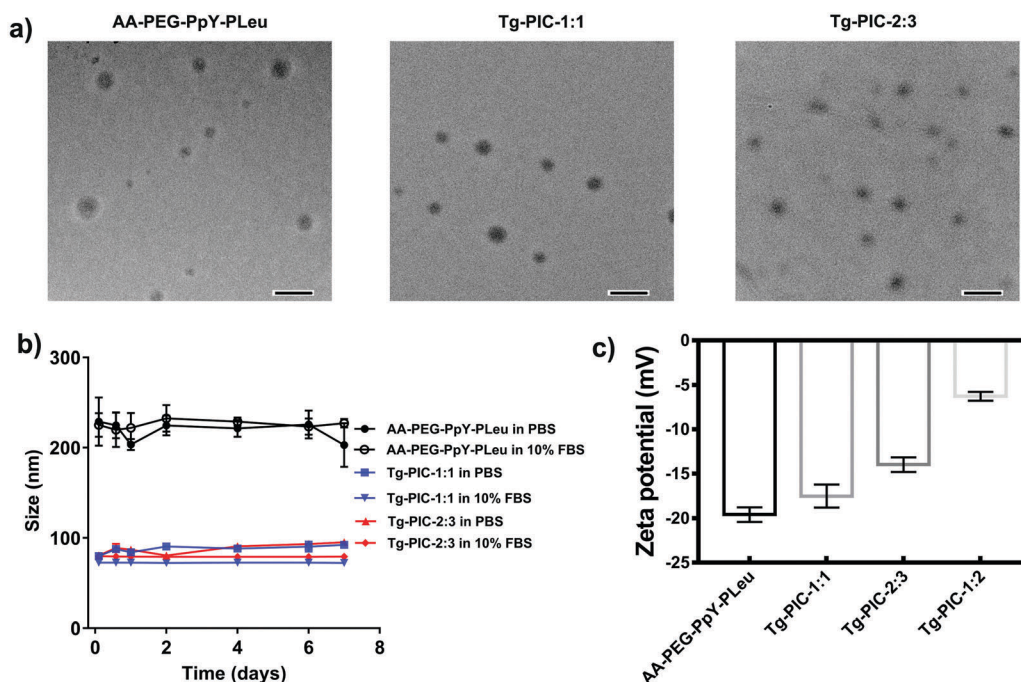


Fig. 3 (a) TEM of AA-PEG-PpY-PLeu and Tg-PICs (P/Gu ratios 1/1, 2/3); scale bar = 200 nm. (b) Hydrodynamic sizes of AA-PEG-PpY-PLeu and Tg-PICs in 1x PBS (pH 7.40) or RPMI1640 with 10% FBS. (c) Zeta potential of AA-PEG-PpY-PLeu and Tg-PICs in 50 mM Tris HCl (pH 7.40).

To further verify the cellular uptake of each material, we examined the cellular platinum level in PC3 cells using ICP-MS. As expected, 4 h of incubation of the positively charged polymer P(DSP-Gu) with PC3 cells at 37 °C resulted in a high cellular platinum concentration of 0.38  $\mu\text{g Pt}$  per  $1.0 \times 10^6$  cells.<sup>66,67</sup>

Again, an anisamide-dependent cellular platinum internalization pattern was clearly observed for the nanocomplexes. Namely, incubation of Tg-PICs (P/Gu ratio 1/1 or 2/3) gave comparable cellular platinum contents to that in P(DSP-Gu) treated cells, whereas incubation with NT-PICs (P/Gu ratio 1/1 or 2/3) led to

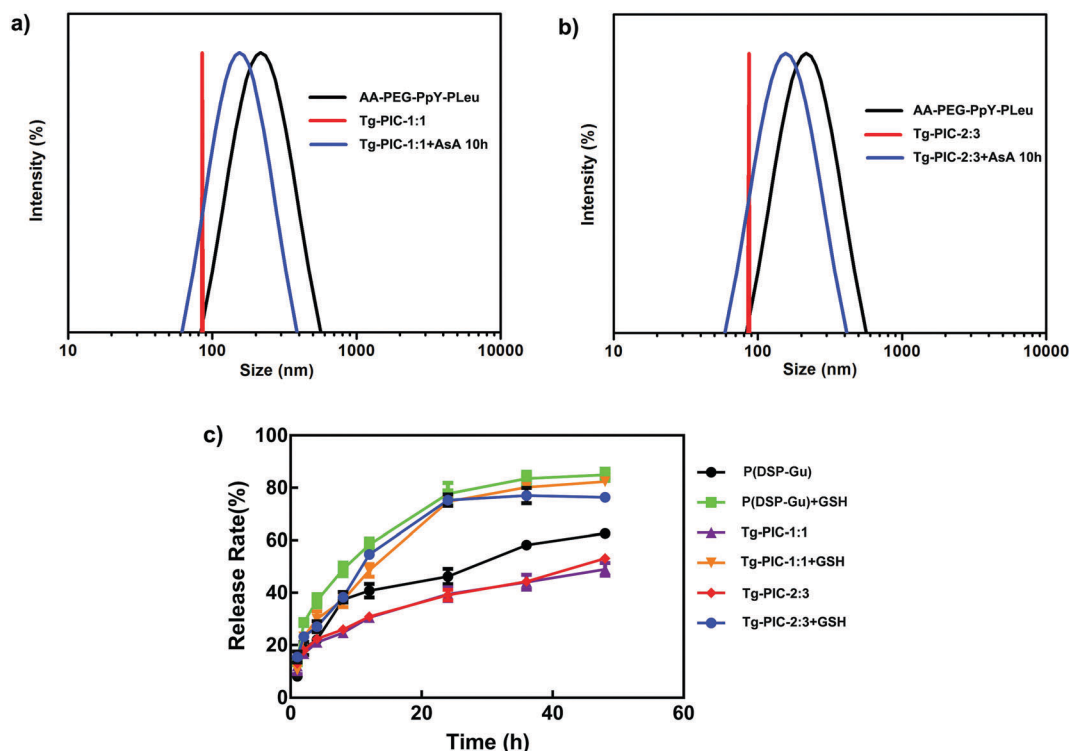


Fig. 4 (a and b) Hydrodynamic sizes of AA-PEG-PpY-PLeu and Tg-PIC in PBS with or without 10 mM AsA; the P/Gu ratios were 1/1 (a) and 2/3 (b). (c) The platinum release kinetics of P(DSP-Gu) and Tg-PICs (P/Gu ratio = 1/1 or 2/3) with or without GSH (2.0 mM) in PBS at 37 °C.

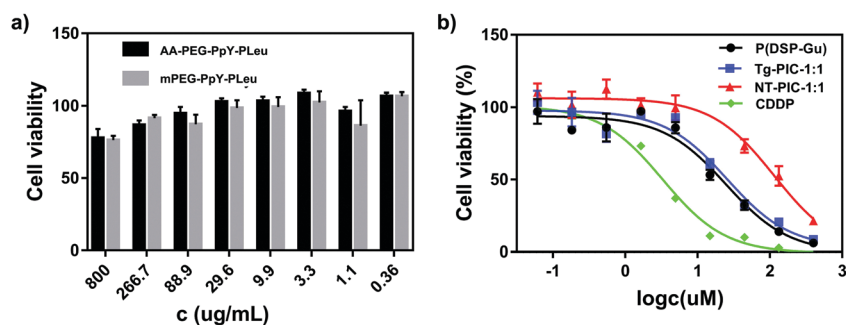


Fig. 5 Cell viability assays of PC3 cells following 72 h of incubation with the carrier polymers AA-PEG-PpY-PLeu and mPEG-PpY-PLeu (a), and the Pt-containing agents CDDP, P(DSP-Gu), Tg-PIC (P/Gu ratio 1/1) and NT-PIC (P/Gu ratio 1/1) (b) at gradient concentrations.

significantly reduced platinum contents in cell lysates ( $\sim 50\%$  less,  $p$  value  $< 0.001$ ). Competitive binding assays by pretreating cells with haloperidol again lowered the platinum uptake, which was in good agreement with the flow cytometry results (Fig. 6c and d). Together, Tg-PICs were selectively internalized by PC3 cells in a ligand-dependent manner.

#### *In vivo* safety and anti-tumor efficacy

The safety and efficacy of the Tg-PICs were further assessed using a xenograft tumor model in which nude mice were subcutaneously inoculated with  $6.0 \times 10^6$  PC3 cells. When the tumors reached  $50 \text{ mm}^3$  (18 days after tumor inoculation) on average (day 0), mice were intravenously administrated PBS, cisplatin (CDDP), P(DSP-Gu), or NT-PIC (P/Gu ratio 2:3) every

other day 8 times (stopped on day 14). On day 20, all mice treated with Tg-PIC (P/Gu = 2:3) therapy still survived, whereas all other treatments led to only 0–60% alive mice (Fig. 7). Notably, apart from P(DSP-Gu), NT-PIC also showed considerable toxicity on day 20 (Fig. 7 and Fig. S20, ESI<sup>†</sup>), which could be attributed to the degradation and release of toxic agents to the reticuloendothelial systems such as the liver. Together, the results indicated that Tg-PIC was well-tolerated at the present dose and safer than cisplatin (CDDP), P(DSP-Gu), and NT-PIC (P/Gu ratio 2:3) due to its active tumor targeting and colloidal stability *in vivo*. Tg-PIC also showed the most prominent tumor growth inhibition with an average relative tumor volume increase of merely 2.6-fold on day 16 (Fig. S20, ESI<sup>†</sup>); in contrast, on the same day the tumors aggressively expanded 32, 7.9, 12.3 and

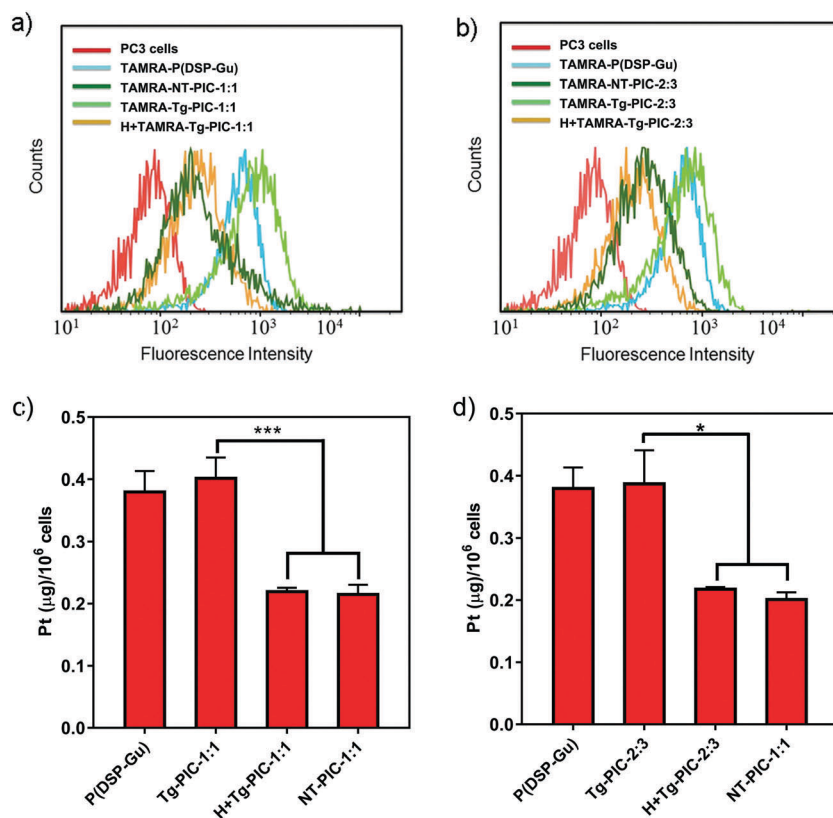


**Fig. 6** (a and b) Flow cytometry analysis of drug internalization in PC3 cells. PC3 cells were treated with mock, TAMRA-labeled P(DSP-Gu), Tg-PIC, NT-PIC or Tg-PIC with 30  $\mu\text{M}$  haloperidol; the P/Gu ratio was 1/1 (a) or 2/3 (b). (c and d) ICP-MS analysis of drug internalization in PC3 cells. PC3 cells were treated with P(DSP-Gu), Tg-PIC, NT-PIC or Tg-PIC with 30  $\mu\text{M}$  haloperidol; the P/Gu ratio was 1/1 (c) or 2/3 (d). The concentration of platinum was determined after 4 h of incubation with different formulations at a Pt concentration of 20  $\mu\text{M}$ . Data were expressed as means  $\pm$  SD from three independent experiments.  $p$  values were determined using two-way ANOVA analysis: \* $p < 0.05$ , \*\*\* $p < 0.001$ .

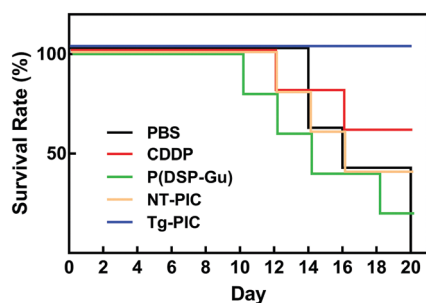


**Fig. 7** Survival curves of mice receiving PBS, CDDP, P(DSP-Gu), NT-PIC, or Tg-PIC (P/Gu = 2:3). Mice bearing PC3 tumors ( $n = 5$ ) of 50  $\text{mm}^3$  were i.v. treated with each therapy every other day 8 times at 2.0 mg Pt per kg dose. All treatments stopped on day 14. Natural death or mice with more than 15% body weight loss or 1000  $\text{mm}^3$  tumors were all counted as mouse death in the survival curves.

10.7-fold in mice infused with PBS, CDDP, P(DSP-Gu), and NT-PIC (P/Gu ratio 2:3), respectively.

## Conclusions

In conclusion, we have designed and synthesized a Pt(IV)-backboned poly-prodrug P(DSP-Gu) with pendant guanidinium

groups. P(DSP-Gu) showed remarkably higher potency than its small molecular precursor DSP and possessed a high and constant drug loading content. By complexing with AA-PEG-PpY-PLeu, we facily constructed targeting nanoparticles, Tg-PICs, that were sub-100 nm in size, stable, and stealthy under physiological conditions. Because of the targeting ability of the anisamide moiety, Tg-PIC showed considerably higher internalization than NT-PIC in the sigma-receptor-positive PC3 cells, which subsequently led to higher potency *in vitro*. *In vivo*, Tg-PIC demonstrated greater antitumor efficacy and less toxicity. Together, our results suggested a new approach for the selective delivery of platinum-based anticancer drugs.

## Experimental section

### Materials

All chemicals were purchased from commercial sources and used as received unless otherwise specified. *cis*-Diamminedichloroplatinum(II) (cisplatin, CDDP) was purchased from HWRK Chem Co., Ltd (Beijing, China). Methoxypolyethylene glycol amine ( $M_w$  5000 Da, mPEG-NH<sub>2</sub>) was purchased from Aladdin Industrial Corporation (China). BocNH-PEG-NH<sub>2</sub> ( $M_w$  5000 Da) was purchased from ToYongBio, Inc. (Shanghai, China). 6-Carboxytetramethylrhodamine succinimidyl ester (6-TAMRA SE) was purchased

from Okeanos Tech. Co., Ltd (Beijing, China). Anhydrous *N,N*-dimethylformamide (DMF) was purchased from Sigma-Aldrich. Pt-NHS,<sup>54</sup> **Gu-11**,<sup>68</sup> **A-1**, **A-2**,<sup>48</sup> pOEt-Tyr-NCA,<sup>69</sup> Leu-NCA<sup>70</sup> were synthesized by following previously reported protocols (Schemes 1 and 2).

### Instrumentation

NMR spectra were recorded on a 400 MHz Bruker ARX400 FT-NMR spectrometer. Fourier transform infrared (FT-IR) spectra were recorded on a Bruker Vector 22 FT-IR spectrometer using a KBr cell with a fixed path length of 0.2 mm for quantification. High resolution electrospray ionization mass spectrometry (HR-ESIMS) analyses were recorded on a Fourier Transform Ion Cyclotron Resonance Mass Spectrometer (APEX IV, Bruker). Inductively Coupled Plasma Mass Spectrometry (ICP-MS) was performed using a NexION 350X (PerkinElmer, USA). Tandem gel permeation chromatography (GPC) experiments were performed on a system equipped with an isocratic pump (Model 1100, Agilent Technology, Santa Clara, CA), a DAWN HELEOS 9-angle laser light scattering detector (Wyatt Technology, Santa Barbara, CA), and an Optilab rEX refractive index detector (Wyatt Technology, Santa Barbara, CA). The temperature of the refractive index detectors was 25 °C. Separations were realized using serially connected size exclusion columns (500, 10<sup>3</sup>, 10<sup>4</sup>, and 10<sup>5</sup> Å Phenogel columns, 5 µm, 7.8 × 300 mm, Phenomenex, Torrance, CA) at 50 °C using DMF containing 0.1 M LiBr as the mobile phase. Dynamic light scattering and zeta potential were measured at 25 °C using a Nanobrook Omni instrument (Brookhaven Instrument Corp. New York, USA), with a laser operating at 640 nm; analyses were performed at an angle of 90° collecting optics. TEM was analyzed using a transmission electron microscope (JEM-2100F, Japan) at an accelerating voltage of 200 kV equipped with a field emission gun, an ultra-high-resolution pole piece, and an ultrathin window JEOL detector. Images were obtained using an OSIS CANTEGA CCD camera. Cyclic voltammetry (CV) was performed on a BASi Epsilon workstation. Confocal images were captured on a Nikon A1R confocal laser scanning microscope system attached to an inverted ECLIPSE Ti (Nikon Corp. Japan). The flow cytometry analysis was performed using a BD LSR Fortessa equipped with 405, 488 and 640 nm lasers (BD Bioscience, USA). Cytotoxicity studies were assayed using an EnSpire<sup>®</sup> Multimode Plate Reader (PerkinElmer, USA).

**Synthesis of Gu-1.** To a stirred MeOH solution (60 mL) containing 6-aminohexanoic acid (1.05 g, 8.0 mmol) and *tert*-butyl (*E*)-(((*tert*-butoxycarbonyl)imino)(1*H*-pyrazol-1-yl)methyl)carbamate (1.24 g, 4.0 mmol) were added DMAP (48.8 mg, 0.4 mmol) and K<sub>2</sub>CO<sub>3</sub> (0.55 g, 4.0 mmol). The reaction mixture was stirred at 30 °C for 2 h and monitored using TLC (PE/EtOAc 5:1). Upon completion of the reaction, the solvent was removed under reduced pressure and the residual solid was dissolved in Et<sub>2</sub>O (100 mL) and washed with citric acid (0.5 M, 60 mL). The aqueous layer was back extracted with Et<sub>2</sub>O (50 mL) and the combined organic phase was washed with brine (80 mL), dried over Na<sub>2</sub>SO<sub>4</sub>, filtered and concentrated. The product was purified using column chromatography on silica gel (PE:EtOAc = 6:1 to 4:1) to give a

colorless oil which solidified upon standing (1.40 g, yield 90%). <sup>1</sup>H NMR (400 MHz, CDCl<sub>3</sub>): δ 8.38 (s, 1H), 3.49–3.40 (m, 2H), 2.37 (t, *J* = 7.4 Hz, 2H), 1.75–1.65 (m, 2H), 1.65–1.55 (m, 2H), 1.51 (s, 9H), 1.50 (s, 9H), 1.42 (m, 2H). MS (ESI): *m/z* (%): 262.0 [M-2*t*Bu + H]<sup>+</sup> (84%), 318.2 [M-Boc + H]<sup>+</sup> (86%), 374.1 [M + H]<sup>+</sup> (100%), 396.2 [M + Na]<sup>+</sup> (35%).

**Synthesis of Gu-2.** To a stirred solution of 6-(2,3-bis(*tert*-butoxycarbonyl)guanidino)hexanoic acid **Gu-1** (1.05 g, 2.82 mmol) and *N,N'*-(azanediylbis(propane-3,1-diyl))bis(2,2,2-trifluoroacetamide) TFA salt **Gu-11** (1.24 g, 2.95 mmol) in DMF (15 mL) were added DIPEA (1.49 mL) and HATU (2.14 g, 5.64 mmol). The resulting solution was stirred at r.t. for 2 h. The reaction mixture was diluted with EtOAc (100 mL), washed with water (2 × 60 mL) and brine (60 mL), dried over Na<sub>2</sub>SO<sub>4</sub>, filtered and concentrated. The crude product was purified using column chromatography on silica gel (PE:EtOAc = 3:1 to 1:2) to obtain a white solid (1.40 g, yield 73%). <sup>1</sup>H NMR (400 MHz, DMSO-*d*<sub>6</sub>) δ 11.49 (s, 1H), 9.45 (t, *J* = 6.2 Hz, 1H), 9.35 (t, *J* = 6.2 Hz, 1H), 8.26 (t, *J* = 5.6 Hz, 1H), 3.29–3.18 (m, *J* = 20.7, 8H), 3.16–3.11 (m, 2H), 2.24 (t, *J* = 7.4 Hz, 2H), 1.78–1.70 (m, 2H), 1.70–1.62 (m, 2H), 1.53–1.48 (m, 13H), 1.39 (s, 9H), 1.30–1.23 (m, 2H). <sup>13</sup>C NMR (101 MHz, DMSO-*d*<sub>6</sub>) δ 172.3, 163.6, 156.7(q), 155.7, 152.6, 117.8, 115.0, 83.3, 78.5, 45.2, 43.0, 38.7, 37.5, 37.3, 32.4, 28.9, 28.5, 28.3, 28.1, 27.3, 26.5, 25.1. MS (ESI): *m/z* (%): 523.3 [M-Boc-*t*Bu + H]<sup>+</sup> (22%), 579.3 [M-Boc + H]<sup>+</sup> (85%), 679.4 [M + H]<sup>+</sup> (100%), 701.4 [M + Na]<sup>+</sup> (49%).

**Synthesis of Gu-3.** To a stirred solution of **Gu-2** (1.40 g, 2.06 mmol) in mixed MeOH (16 mL) and water (8 mL) was added K<sub>2</sub>CO<sub>3</sub> (712 mg, 5.16 mmol) in one portion. The resulting solution was stirred at 25 °C for 12 h. The reaction mixture was concentrated to remove the methanol and diluted with water (30 mL), and extracted with CHCl<sub>3</sub>/*i*-PrOH (v/v 3:1) (2 × 80 mL), and the combined organic phase was dried over Na<sub>2</sub>SO<sub>4</sub>, filtered and concentrated. The crude product was purified using column chromatography on silica gel (DCM:MeOH 10:1 in the beginning, followed by DCM:MeOH:NH<sub>4</sub>OH = 75:25:5). The pure fractions were combined and concentrated to remove most of the organic solvent. The residual was diluted with water (10 mL) and lyophilized to obtain a white powder (650 mg, yield 63%). <sup>1</sup>H NMR (400 MHz, CD<sub>3</sub>OD) δ 3.42 (t, *J* = 6.2 Hz, 2H), 3.39–3.33 (m, 4H), 2.68 (t, *J* = 7.0 Hz, 2H), 2.63 (t, *J* = 6.8 Hz, 2H), 2.41 (t, *J* = 7.5 Hz, 2H), 1.80–1.58 (m, 8H), 1.52 (s, 9H), 1.47 (s, 9H), 1.44–1.37 (m, 2H). <sup>13</sup>C NMR (101 MHz, CD<sub>3</sub>OD) δ 174.2, 163.2, 156.2, 152.9, 83.1, 78.9, 45.5, 42.5, 40.3, 38.5, 38.0, 32.3, 31.5, 29.6, 28.6, 27.2, 26.9, 26.2, 25.0. HRMS (ESI): *m/z*: calcd for C<sub>23</sub>H<sub>47</sub>N<sub>6</sub>O<sub>5</sub> [M + H]<sup>+</sup>: 487.36079; found: 487.35927 (found), error 3.1 ppm.

**Synthesis of Gu-4.** A 5-mL vial was charged with NHS-Pt-NHS (218.5 mg, 0.3 mmol), **Gu-3** (146.9 mg, 0.30 mmol) and DIPEA (9.9 µL, 0.2 eq.) in dry DMF (0.9 mL). The vial was flushed with nitrogen and stirred at room temperature for 72 h in the dark. The crude product was precipitated and washed with Et<sub>2</sub>O (40 mL, twice), and dried under high vacuum to yield a yellow solid (330 mg), which was used directly in the next step without further purification.

**Synthesis of polymer P(DSP-Gu).** The crude **Gu-4** (330 mg) obtained from the last step was dissolved in DCM (10 mL),

to which was added TFA (2 mL). The resulting solution was stirred at 25 °C for 12 h in the dark. The reaction mixture was evaporated and co-evaporated with DCM once. The residue was dissolved in deionized (DI) water (25 mL) and con. HCl aq. (270  $\mu$ L, 10 eq.) was added. The solution was stirred at r.t. for 10 min, filtered (through a 0.22  $\mu$ m water phase filter), and then dialysed against DI water (MWCO 3500 Da) at 4 °C in the dark for 12 h before lyophilization to yield a white solid (150 mg, yield 61%). <sup>1</sup>H NMR (400 MHz, D<sub>2</sub>O):  $\delta$  3.47–3.32 (m), 3.29–3.10 (m), 2.79–2.70 (m), 2.57–2.46 (m), 2.43 (m), 1.82–1.78 (m), 1.71–1.56 (m), 1.42–1.38 (m). Elemental analysis by ICP-MS: Pt (wt%) calc. 23.8%; obtained 22.2%.

**Synthesis of TAMRA-P(DSP-Gu).** A 5-mL vial was charged with Pt–NHS (145.6 mg, 0.20 mmol), Gu-3 (97.2 mg, 0.20 mmol), and DIPEA (6.6  $\mu$ L, 0.2 eq.) in dry DMF (0.6 mL). The vial was flushed with nitrogen and stirred at room temperature for 72 h in the dark followed by the addition of an aliquot of Gu-3 (9.7 mg, 0.02 mmol, 0.10 eq.) and stirring at r.t. for 24 h to obtain an amine-capped polymer. To the resulting polymer was then added 6-TAMRA-SE (21.1 mg, 0.04 mmol, 0.20 eq.) and the mixture was stirred for another 24 h for TAMRA labeling. The crude product was precipitated in Et<sub>2</sub>O (40 mL, twice) and dried under high vacuum. The resulting solid was dissolved in DCM (7.5 mL), to which was added TFA (1.5 mL) for deprotection. The resulting solution was stirred at 25 °C for 12 h in the dark. The reaction mixture was evaporated and the residue was dissolved in mixed DI water (15 mL) and con. HCl aq. (180  $\mu$ L), stirred at r.t. for 10 min, filtered, and then dialyzed against DI water (MWCO 3500 Da) at 4 °C in the dark for 12 h before lyophilization to obtain a purple solid (70 mg, yield 43%).

**Synthesis of A-1.** Boc-HN-PEG-NH<sub>2</sub> (*M<sub>w</sub>* 5000 Da, 510 mg, 0.10 mmol) and anisic acid (121.5 mg, 0.80 mmol) were dissolved in DCM (8 mL). DIPEA (66  $\mu$ L, 0.40 mmol) and *N,N'*-diisopropylcarbodiimide (DIC) (125  $\mu$ L, 0.80 mmol) were added to the mixture and stirred at r.t. for 26 h. The reaction mixture was concentrated to 4 mL and precipitated in Et<sub>2</sub>O (80 mL), washed with Et<sub>2</sub>O (twice), and dried under high vacuum to give A-1 as a white solid (510 mg, 95%). <sup>1</sup>H NMR (400 MHz, CDCl<sub>3</sub>)  $\delta$  7.79 (d), 6.92 (d), 3.85 (s), 3.82 (t), 3.75–3.60 (m), 3.54 (t), 3.48 (t), 3.31 (t), 1.45 (s).

**Synthesis of A-2.** A-1 (500 mg) was dissolved in DCM (4 mL), to which was added TFA (2 mL) in one portion. The reaction mixture was stirred at r.t. for 2 h and then precipitated in Et<sub>2</sub>O (80 mL). The resulting solid was dissolved in saturated NaCl/KCl aqueous solution (*v/v* = 1/1) and extracted with DCM (3  $\times$  10 mL). The combined organic phase was dried over Na<sub>2</sub>SO<sub>4</sub>, filtered and concentrated to 2 mL volume, precipitated in Et<sub>2</sub>O (40 mL), washed with Et<sub>2</sub>O, and dried under high vacuum to give A-2 as a white solid (350 mg, 70%). <sup>1</sup>H NMR (400 MHz, CDCl<sub>3</sub>)  $\delta$  7.79 (d), 6.92 (d), 3.87–3.81 (m), 3.65 (s), 3.47 (d), 3.19 (br s).

**Synthesis of A-3.** A 20-mL vial was charged with pOEt-Tyr-NCA (309 mg, 0.90 mmol) in dry DMF (2.5 mL), followed by the macro-initiator A-2 (78 mg, 0.015 mmol). The reaction mixture was stirred at r.t. for 24 h in a glovebox and monitored using FT-IR. Upon the consumption of pOEt-Tyr-NCA, Leu-NCA (58.5 mg, 0.37 mmol) was added to the reaction mixture and

the mixture was stirred at r.t. for another 16 h. The reaction mixture was precipitated in Et<sub>2</sub>O (80 mL), washed with Et<sub>2</sub>O (twice), and dried in a vacuum oven (50 °C) to give A-3 as a white solid (270 mg, yield 91%).

**Synthesis of AA-PEG-PpY-PLeu and mPEG-PpY-PLeu.** To a solution of A-3 (300 mg) in dry CHCl<sub>3</sub> (6.0 mL) was added bromotrimethylsilane (1.35 mL, 10.1 mmol) and triethylamine (1.13 mL, 7.9 mmol). The mixture was heated up to 60 °C and stirred for 8 h. The solvent was removed under vacuum and the residue was dissolved in DI water (20 mL) with the pH adjusted to near neutral using 1 N NaOH. The crude product was then purified by dialysis (3500 Da MWCO) against 0.1 M sodium chloride (2 L  $\times$  2 times) for 8 h, followed by against water for a total of 9 h (2 L  $\times$  3 times). The remaining solution was freeze dried to afford AA-PEG-PpY-PLeu as a fluffy, brownish powder (270 mg, yield 90%).

mPEG-PpY-PLeu was synthesized by the same method described above except for using mPEG-NH<sub>2</sub> to replace A-3 as the initiator.

### Electrochemistry

Cyclic voltammetry (CV) was performed using degassed phosphate-buffer (10 mM, pH 6.0 or 7.4) with 0.1 M KCl as the supporting electrolyte. A glassy carbon electrode and platinum wire were used as the working electrode and the counter electrode, respectively. All potentials were represented using Ag/AgCl (saturated) as the reference electrode. The platinum concentration of the polymer was set as 1.0 mM at varying scan rates between 50 and 350 mV s<sup>-1</sup>. The electrolyte solution was bubbled with nitrogen for 20 minutes before each measurement.

### Preparation of PICs

The amphiphilic carrier polymer, AA-PEG-PpY-PLeu or mPEG-PpY-PLeu, was dissolved in PBS (1 $\times$ , pH 7.40) or 10% FBS-1640 medium at a pY concentration of 4.0 mM and sonicated for 15 min at room temperature. P(DSP-Gu) solution (4.0 mM based on Pt) was prepared by dissolving it in PBS (1 $\times$ , pH 7.40) and vortexed for 30 s. The PICs (Tg-PIC or NT-PIC) were prepared by mixing the solution of AA-PEG-PpY-PLeu or mPEG-PpY-PLeu with P(DSP-Gu) at varied volume ratios followed by vortexing for 30 s. For DLS and TEM tests, the mixtures were diluted with PBS or 10% FBS-1640 medium to obtain a Pt(IV) final concentration of 0.2–0.3 mM. The zeta potential test was performed in Tris HCl (50 mM, pH 7.40) buffer with a Pt(IV) concentration of 0.20 mM.

### Degradation of Tg-PICs under reducing conditions

To the Tg-PIC solution in PBS (P/G ratio of 1/1 or 2/3, 1.0 mL, 0.3 mM based on Pt) was added sodium ascorbate (10.0 mM, pH 7.40). The mixture was incubated at 37 °C for 10 h in the dark. An aliquot of the solution was withdrawn from the solution for DLS analysis.

### Platinum release assays measured using ICP-MS

P(DSP-Gu) or Tg-PICs (1.0 mM Pt, 1.0 mL) in PBS were placed in a dialysis bag (MWCO 3 kDa) and dialyzed against 99 mL of PBS (pH 7.4) at 37 °C. An aliquot of PBS (1.0 mL) was withdrawn from the medium outside the dialysis tube at specified time

intervals for ICP-MS analysis. To maintain the overall volume at 100 mL, 1.0 mL of fresh PBS was replenished each time.

### Cells and animals

Prostate cancer cells (PC3) were a generous gift from Prof. Fan Chunhai (Shanghai Institute of Applied Physics, Chinese Academy of Sciences). PC3 cells were cultured in RPMI 1640 (Corning, Manassas, USA) and supplemented with 10% FBS (Gibco), 100 U mL<sup>-1</sup> penicillin and 100 U mL<sup>-1</sup> streptomycin (Corning, Manassas, USA) in a humidified atmosphere containing 5% CO<sub>2</sub> at 37 °C. Six-week-old male BALB/c mice were ordered from Vital River Laboratories (Beijing, China). All animal experiments were performed in compliance with the Guide for the Care and Use of Laboratory Animals and were approved by the Experimental Animal Ethics Committee in Beijing.

### *In vitro* cell uptake assays using ICP-MS

1.5 × 10<sup>6</sup> PC3 cells were seeded in Corning<sup>®</sup> 100 mm TC-Treated Culture Dishes and incubated for 24 h before the experiment. The cells were treated with P(DSP-Gu), Tg-PICs (P/G ratio = 1/1 or 2/3), or NT-PICs (P/G ratio = 1/1 or 2/3) at 37 °C for 4 h (20 μM platinum). Afterwards, the cells were washed with heparin sodium (1.0 mg mL<sup>-1</sup>, 1.0 mL × 2) and PBS buffer (1.0 mL × 2), trypsinized, and the cell numbers were counted. The cells were then digested by HNO<sub>3</sub> and the intracellular Pt contents were measured using ICP-MS.

For competitive inhibition experiments, PC3 cells were pretreated with 30 μM haloperidol for 3 h to block the sigma receptors on the cell surface, and the media were aspirated and replaced by fresh culture media before treatment of Tg-PICs.

### Cell viability assay

PC3 cells in the exponential growth phase were seeded into a blank 96-well plate at a density of 3000 cells per well for 24 h prior to the assay. The culture medium was removed and the cells were treated with P(DSP-Gu), Tg-PICs (P/G ratio = 1/1 or 2/3), or NT-PICs (P/G ratio = 1/1 or 2/3) in a fresh medium at gradient concentrations (*n* = 3). After incubation for 72 h, the relative cell viabilities were monitored using a CellTiter-Blue<sup>®</sup> Cell Viability Assay (Promega, USA) by following the manufacturer's protocol. IC<sub>50</sub>s were calculated by GraphPad Prism version 5 using the log(inhibitor) vs. response regression method.

### Confocal laser scanning microscopy analysis

PC3 cells in the exponential growth phase were seeded in glass bottomed culture chambers (20 mm, Nest) at a density of 3 × 10<sup>4</sup> cells per well. The cells were incubated at 37 °C in a humidified atmosphere containing 5% CO<sub>2</sub> for 48 h. The cells were treated with fresh medium (1.0 mL) containing TAMRA-labeled P(DSP-Gu), Tg-PICs (P/G ratio = 1/1 or 2/3), or NT-PICs (P/G ratio = 1/1 or 2/3) (20 μM based on platinum) for 4 h. The cells were washed sequentially with heparin sodium (1.0 mg mL<sup>-1</sup>, 1.0 mL × 2), and PBS buffer (1.0 mL × 1) and stained with Hoechst 33342 (Life Technologies Inc. Carlsbad, USA) for 20 min at 37 °C in the dark. The cells were imaged in cell culture medium (1.0 mL) after rinsing with 1 × PBS (1.0 mL) three times.

### Cell uptake analyzed by flow cytometry

Cells (1.0 × 10<sup>5</sup> per well) were seeded in a 6-well plate and incubated for 24 h at 37 °C. Fresh medium containing P(DSP-Gu), Tg-PICs (P/G ratio = 1/1 or 2/3), or NT-PICs (P/G ratio = 1/1 or 2/3) was then supplemented to the cells (with 20 μM platinum concentration). After 4 h of incubation, the cells were washed sequentially with heparin sodium (1.0 mg mL<sup>-1</sup>, 1.0 mL × 2) and PBS buffer (1.0 mL × 2). The cells were then digested with 0.05% trypsin, centrifuged, and resuspended in PBS for flow cytometry analysis. For competitive inhibition experiments, PC3 cells were pretreated with 30 μM haloperidol for 3 h to block the sigma receptors on the cell surface, and the media were aspirated and replaced by fresh culture media before the PIC treatment.

### *In vivo* anti-tumor efficacy

The human prostate carcinoma PC3 xenograft tumor model was established by subcutaneous injection of PC3 cells (6.0 × 10<sup>6</sup> in 100 μL PBS) into the right flank of each BALB/c-nu mouse. When the tumor size reached 50 mm<sup>3</sup> (18 days after tumor inoculation), the mice began to receive PBS, cisplatin (CDDP), P(DSP-Gu), and NT-PIC (P/Gu ratio 2:3) treatments at a 2 mg kg<sup>-1</sup> platinum dose once every other day. The tumor size and body weight of the mice were recorded once every other day.

The tumor volume was calculated using the following formula:

$$V = L \cdot W^2 / 2$$

The relative tumor volume was calculated using the formula:  $R = V/V_0$ , where  $V_0$  is the average tumor volume on day 0 (the administration date). The relative body weight ( $R$ ) was calculated using the formula:  $R = W/W_0$ , where  $W_0$  is the body weight before administration.

## Conflicts of interest

There are no conflicts to declare.

## Acknowledgements

This work was financially supported by the National Key Research and Development Program of China (No. 2016YFA0201400) and State High-Tech Development Program of China (863 Program No. 2015AA020941). H. L. acknowledges the grants from the National Natural Science Foundation of China (NSFC21434008), and the Open Funding Project of the State Key Laboratory of Biochemical Engineering (No. 2015KF-01). S.-L. was supported in part by the China Postdoctoral Science Foundation (No. 2016M600847) and the Postdoctoral Fellowship of Peking-Tsinghua Center for Life Sciences.

## References

- 1 J. D. Byrne, T. Betancourt and L. Brannon-Peppas, *Adv. Drug Delivery Rev.*, 2008, **60**, 1615–1626.
- 2 R. Duncan and M. J. Vicent, *Adv. Drug Delivery Rev.*, 2010, **62**, 272–282.

- 3 V. P. Torchilin, *Nat. Rev. Drug Discovery*, 2014, **13**, 813–827.
- 4 F. Li, J. Lu, X. Kong, T. Hyeon and D. Ling, *Adv. Mater.*, 2017, **29**, 1605897.
- 5 J. Li, Z. Ge and S. Liu, *Chem. Commun.*, 2013, **49**, 6974–6976.
- 6 X. He, J. Fan, F. Zhang, R. Li, K. A. Pollack, J. E. Raymond, J. Zou and K. L. Wooley, *J. Mater. Chem. B*, 2014, **2**, 8123–8130.
- 7 M. Huo, J. Yuan, L. Tao and Y. Wei, *Polym. Chem.*, 2014, **5**, 1519–1528.
- 8 D. Liu, C. Poon, K. Lu, C. He and W. Lin, *Nat. Commun.*, 2014, **5**, 4182.
- 9 J. Chen, J. Ding, Y. Wang, J. Cheng, S. Ji, X. Zhuang and X. Chen, *Adv. Mater.*, 2017, **29**, 1701170.
- 10 Z. Dong, L. Feng, W. Zhu, X. Sun, M. Gao, H. Zhao, Y. Chao and Z. Liu, *Biomaterials*, 2016, **110**, 60–70.
- 11 F. Fan, L. Wang, F. Li, Y. Fu and H. Xu, *ACS Appl. Mater. Interfaces*, 2016, **8**, 17004–17010.
- 12 W. Sun, S. Li, B. Häupler, J. Liu, S. Jin, W. Steffen, U. S. Schubert, H. J. Butt, X. J. Liang and S. Wu, *Adv. Mater.*, 2017, **29**, 1603702.
- 13 Q. Hu, W. Sun, C. Wang and Z. Gu, *Adv. Drug Delivery Rev.*, 2016, **98**, 19–34.
- 14 S. Kaur, C. Prasad, B. Balakrishnan and R. Banerjee, *Biomater. Sci.*, 2015, **3**, 955–987.
- 15 M. Elsbahy, G. S. Heo, S.-M. Lim, G. Sun and K. L. Wooley, *Chem. Rev.*, 2015, **115**, 10967–11011.
- 16 J. Kim, S. Pramanick, D. Lee, H. Park and W. J. Kim, *Biomater. Sci.*, 2015, **3**, 1002–1017.
- 17 T. C. Johnstone, K. Suntharalingam and S. J. Lippard, *Chem. Rev.*, 2016, **116**, 3436–3486.
- 18 H. Waldmann, E. Valeur, S. M. Guéret, H. Adihou, R. Gopalakrishnan, M. Lemurell, T. N. Grossmann and A. T. Plowright, *Angew. Chem., Int. Ed.*, 2017, **56**, 10294–10323.
- 19 H. Sun and Y. Zu, *Small*, 2015, **11**, 2352–2364.
- 20 J. C. Evans, M. Malhotra, J. Guo, J. P. O'Shea, K. Hanrahan, A. O'Neill, W. D. Landry, B. T. Griffin, R. Darcy, R. W. Watson and C. M. O'Driscoll, *Nanomedicine*, 2016, **12**, 2341–2351.
- 21 Q. Cheng and Y. Liu, *Wiley Interdiscip. Rev.: Nanomed. Nanobiotechnol.*, 2017, **9**, e1410.
- 22 Y. Takahashi, M. Nishikawa and Y. Takakura, *Adv. Drug Delivery Rev.*, 2009, **61**, 760–766.
- 23 M. S. Shim and Y. J. Kwon, *Adv. Drug Delivery Rev.*, 2012, **64**, 1046–1059.
- 24 H. Yin, R. L. Kanasty, A. A. Eltoukhy, A. J. Vegas, J. R. Dorkin and D. G. Anderson, *Nat. Rev. Genet.*, 2014, **15**, 541–555.
- 25 S. Shen, C.-Y. Sun, X.-J. Du, H.-J. Li, Y. Liu, J.-X. Xia, Y.-H. Zhu and J. Wang, *Biomaterials*, 2015, **70**, 71–83.
- 26 C.-Y. Sun, S. Shen, C.-F. Xu, H.-J. Li, Y. Liu, Z.-T. Cao, X.-Z. Yang, J.-X. Xia and J. Wang, *J. Am. Chem. Soc.*, 2015, **137**, 15217–15224.
- 27 C. B. He, C. Poon, C. Chan, S. D. Yamada and W. B. Lin, *J. Am. Chem. Soc.*, 2016, **138**, 6010–6019.
- 28 C.-F. Xu, H.-B. Zhang, C.-Y. Sun, Y. Liu, S. Shen, X.-Z. Yang, Y.-H. Zhu and J. Wang, *Biomaterials*, 2016, **88**, 48–59.
- 29 X. Xu, J. Wu, Y. Liu, M. Yu, L. Zhao, X. Zhu, S. Bhasin, Q. Li, E. Ha, J. Shi and O. C. Farokhzad, *Angew. Chem., Int. Ed.*, 2016, **55**, 7091–7094.
- 30 A. J. Harnoy, I. Rosenbaum, E. Tirosh, Y. Ebenstein, R. Shaharabani, R. Beck and R. J. Amir, *J. Am. Chem. Soc.*, 2014, **136**, 7531–7534.
- 31 C.-Y. Sun, Y. Liu, J.-Z. Du, Z.-T. Cao, C.-F. Xu and J. Wang, *Angew. Chem., Int. Ed.*, 2016, **55**, 1010–1014.
- 32 X.-D. Xu, Y.-J. Cheng, J. Wu, H. Cheng, S.-X. Cheng, R.-X. Zhuo and X.-Z. Zhang, *Biomaterials*, 2016, **76**, 238–249.
- 33 X. Fang, W. Jiang, Y. Huang, F. Yang and T. Chen, *J. Mater. Chem. B*, 2017, **5**, 944–952.
- 34 X. Xu, P. E. Saw, W. Tao, Y. Li, X. Ji, S. Bhasin, Y. Liu, D. Ayyash, J. Rasmussen, M. Huo, J. Shi and O. C. Farokhzad, *Adv. Mater.*, 2017, **29**, 1700141.
- 35 H. Song, H. Xiao, Y. Zhang, H. Cai, R. Wang, Y. Zheng, Y. Huang, Y. Li, Z. Xie, T. Liu and X. Jing, *J. Mater. Chem. B*, 2013, **1**, 762–772.
- 36 C. Zheng, M. Zheng, P. Gong, J. Deng, H. Yi, P. Zhang, Y. Zhang, P. Liu, Y. Ma and L. Cai, *Biomaterials*, 2013, **34**, 3431–3438.
- 37 J. J. Wilson and S. J. Lippard, *Chem. Rev.*, 2014, **114**, 4470–4495.
- 38 X.-Z. Yang, X.-J. Du, Y. Liu, Y.-H. Zhu, Y.-Z. Liu, Y.-P. Li and J. Wang, *Adv. Mater.*, 2014, **26**, 931–936.
- 39 T. Li, M. Smet, W. Dehaen and H. Xu, *ACS Appl. Mater. Interfaces*, 2016, **8**, 3609–3614.
- 40 Y. Hou, Y. Wang, R. Wang, W. Bao, X. Xi, Y. Sun, S. Yang, W. Wei and H. Lu, *ACS Appl. Mater. Interfaces*, 2017, **9**, 17757–17768.
- 41 R. Zhang, X. Song, C. Liang, X. Yi, G. Song, Y. Chao, Y. Yang, K. Yang, L. Feng and Z. Liu, *Biomaterials*, 2017, **138**, 13–21.
- 42 E. G. Stanzl, B. M. Trantow, J. R. Vargas and P. A. Wender, *Acc. Chem. Res.*, 2013, **46**, 2944–2954.
- 43 C. J. McKinlay, R. M. Waymouth and P. A. Wender, *J. Am. Chem. Soc.*, 2016, **138**, 3510–3517.
- 44 P. Zhang, Y. Wang, J. Lian, Q. Shen, C. Wang, B. Ma, Y. Zhang, T. Xu, J. Li, Y. Shao, F. Xu and J.-J. Zhu, *Adv. Mater.*, 2017, **29**, 1702311.
- 45 S.-S. Han, Z.-Y. Li, J.-Y. Zhu, K. Han, Z.-Y. Zeng, W. Hong, W.-X. Li, H.-Z. Jia, Y. Liu, R.-X. Zhuo and X.-Z. Zhang, *Small*, 2015, **11**, 2543–2554.
- 46 R. Banerjee, P. Tyagi, S. Li and L. Huang, *Int. J. Cancer*, 2004, **112**, 693–700.
- 47 O. Nakagawa, X. Ming, L. Huang and R. L. Juliano, *J. Am. Chem. Soc.*, 2010, **132**, 8848–8849.
- 48 L. Miao, S. Guo, J. Zhang, W. Y. Kim and L. Huang, *Adv. Funct. Mater.*, 2014, **24**, 6601–6611.
- 49 A. Dasargyri, P. Hervella, A. Christiansen, S. T. Proulx, M. Detmar and J.-C. Leroux, *J. Controlled Release*, 2016, **224**, 229–238.
- 50 K. A. Fitzgerald, K. Rahme, J. Guo, J. D. Holmes and C. M. O'Driscoll, *J. Mater. Chem. B*, 2016, **4**, 2242–2252.
- 51 A. Dasargyri, C. D. Kümin and J.-C. Leroux, *Adv. Mater.*, 2017, **29**, 1603451.
- 52 W. Yang, Y. Zou, F. Meng, J. Zhang, R. Cheng, C. Deng and Z. Zhong, *Adv. Mater.*, 2016, **28**, 8234–8239.
- 53 J. Yang, W. W. Liu, M. H. Sui, J. B. Tang and Y. Q. Shen, *Biomaterials*, 2011, **32**, 9136–9143.

- 54 S.-L. Li, Y. Hou, Y. Hu, J. Yu, W. Wei and H. Lu, *Biomater. Sci.*, 2017, **5**, 1558–1566.
- 55 S. Dhar, W. L. Daniel, D. A. Giljohann, C. A. Mirkin and S. J. Lippard, *J. Am. Chem. Soc.*, 2009, **131**, 14652–14653.
- 56 L. Ellis, H. Er and T. Hambley, *Aust. J. Chem.*, 1995, **48**, 793–806.
- 57 S. Choi, C. Filotto, M. Bisanzo, S. Delaney, D. Lagasee, J. L. Whitworth, A. Jusko, C. Li, N. A. Wood, J. Willingham, A. Schwenker and K. Spaulding, *Inorg. Chem.*, 1998, **37**, 2500–2504.
- 58 S. Dhar, Z. Liu, J. Thomale, H. Dai and S. J. Lippard, *J. Am. Chem. Soc.*, 2008, **130**, 11467–11476.
- 59 Y. Hu, L. Zhang, Y. Cao, H. Ge, X. Jiang and C. Yang, *Biomacromolecules*, 2004, **5**, 1756–1762.
- 60 Y.-Y. Li, S.-H. Hua, W. Xiao, H.-Y. Wang, X.-H. Luo, C. Li, S.-X. Cheng, X.-Z. Zhang and R.-X. Zhuo, *J. Mater. Chem.*, 2011, **21**, 3100–3106.
- 61 J. Mao, Y. Li, T. Wu, C. Yuan, B. Zeng, Y. Xu and L. Dai, *ACS Appl. Mater. Interfaces*, 2016, **8**, 17109–17117.
- 62 N. Kolishetti, S. Dhar, P. M. Valencia, L. Q. Lin, R. Karnik, S. J. Lippard, R. Langer and O. C. Farokhzad, *Proc. Natl. Acad. Sci. U. S. A.*, 2010, **107**, 17939–17944.
- 63 R. K. Pathak and S. Dhar, *J. Am. Chem. Soc.*, 2015, **137**, 8324–8327.
- 64 K. Kim and W. G. Lee, *J. Mater. Chem. B*, 2017, **5**, 2726–2738.
- 65 J. Tian, Y. Min, Z. Rodgers, K. M. Au, C. T. Hagan, M. Zhang, K. Roche, F. Yang, K. Wagner and A. Z. Wang, *J. Mater. Chem. B*, 2017, **5**, 6049–6057.
- 66 N. Bertrand, J. Wu, X. Xu, N. Kamaly and O. C. Farokhzad, *Adv. Drug Delivery Rev.*, 2014, **66**, 2–25.
- 67 H.-J. Li, J.-Z. Du, J. Liu, X.-J. Du, S. Shen, Y.-H. Zhu, X. Wang, X. Ye, S. Nie and J. Wang, *ACS Nano*, 2016, **10**, 6753–6761.
- 68 R. A. Kramer, M. C. Bröhmer, N. V. Forkel and W. Bannwarth, *Eur. J. Org. Chem.*, 2009, 4273–4283.
- 69 Y. Sun, Y. Hou, X. Zhou, J. Yuan, J. Wang and H. Lu, *ACS Macro Lett.*, 2015, **4**, 1000–1003.
- 70 C. D. Vacogne and H. Schlaad, *Chem. Commun.*, 2015, **51**, 15645–15648.